

When ControlNet Meets Inexplicit Masks: A Case Study of ControlNet on its Contour-following Ability

Wenjie Xuan, Yufei Xu, Shanshan Zhao, Chaoyue Wang
Juhua Liu*, Bo Du*, Dacheng Tao

{dreamxwj, liujuhua, dubo}@whu.edu.cn, yuxu7116@uni.sydney.edu.au
{sshan.zhao00, dacheng.tao}@gmail.com, chaoyue.wang@outlook.com

Abstract

ControlNet excels at creating content that closely matches precise contours in user-provided masks. However, when these masks contain noise, as a frequent occurrence with non-expert users, the output would include unwanted artifacts. This paper first highlights the crucial role of controlling the impact of these inexplicit masks with diverse deterioration levels through in-depth analysis. Subsequently, to enhance controllability with inexplicit masks, an advanced Shape-aware ControlNet consisting of a deterioration estimator and a shape-prior modulation block is devised. The deterioration estimator assesses the deterioration factor of the provided masks. Then this factor is utilized in the modulation block to adaptively modulate the model’s contour-following ability, which helps it dismiss the noise part in the inexplicit masks. Extensive experiments prove its effectiveness in encouraging ControlNet to interpret inaccurate spatial conditions robustly rather than blindly following the given contours. We showcase application scenarios like modifying shape priors and composable shape-controllable generation. Codes are available.

1 Introduction

Text-to-Image (T2I) generation techniques [Saharia *et al.*, 2022; Ramesh *et al.*, 2022; Ramesh *et al.*, 2021] have greatly changed the content creation area with high-fidelity synthesized images. By generating content following user-provided guidance like contours and shapes, ControlNet [Zhang *et al.*, 2023a] stands out for its prominent capability of spatial control over T2I diffusion models and has become an indispensable tool for creation. The shape guidance always takes the format of segmentation masks, where the details of the contours and positions are perfectly reserved as shown in Fig. 1. However, such good *contour-following ability*¹ of ControlNet may cause artifacts when there exists noise in the mask, especially for non-expert users that have difficulty in providing accurate masks. Unfortunately, its performance on inexplicit

*Corresponding Author

¹The ability to preserve contours of the conditional inputs.

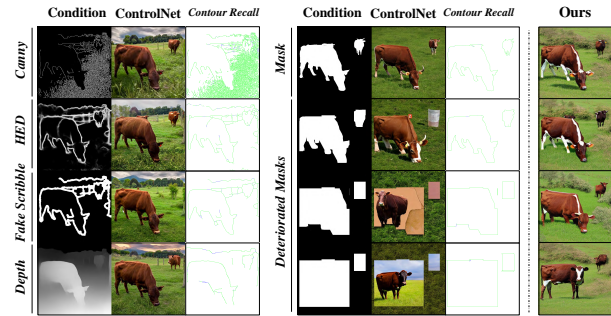


Figure 1: ControlNet tends to preserve contours for spatial controllable generation over multi-modal control inputs, where **green** denotes recalled contours and **blue** denotes missing ones. However, inexplicit masks cause catastrophic degradation of image fidelity and realism. This paper largely enhances its robustness in interpreting inexplicit masks with inaccurate contours.

masks with inaccurate contours remains under-explored, and studies on how to employ inexplicit masks are ignored in current works. This issue hinders non-expert users from creating better images through ControlNet.

To better assist non-expert users in generating satisfactory images, this paper focuses on utilizing inexplicit masks during the generation process. We first analyze the most important property, *i.e.*, the contour-following ability, on the inexplicit mask-guided generation process through deteriorating masks and tuning hyperparameters. Specifically, we study this property quantitatively and reveal preliminary analyses on two key areas: 1) its performance on conditional masks at varying precision levels, and 2) the influence of hyperparameters on this property. One of the main findings is that masks with inaccurate contours would cause artifacts due to strong contour instructions. In other words, the contour-following ability implicitly assumes that *the conditional inputs align with the shape priors of specific objects*. Otherwise, it would cause artifacts or violate the spatial control in synthesized images as shown in Fig. 1. Given that precise conditional images are typically image-oriented (*e.g.*, human annotation or those extracted from reference images by offline detectors) or expert-provided (*e.g.*, artists), it constrains creation within the boundaries of existing images and experts. Obtaining precise control inputs can be cumbersome and challenging for non-

experts. This fact largely restricts creation through scribbles, thus hindering broad applications of ControlNet.

While an intuitive solution is to adjust hyperparameters to achieve satisfactory results, finding the optimal setting can be challenging. Besides, this strategy usually entails a trade-off between image fidelity and spatial control. Based on this observation, we improve ControlNet with the awareness of shape priors, namely Shape-aware ControlNet, which alleviates the impact of strong contour instructions and shows advances in robust interpretation of inexplicit masks. Specifically, our improvements comprise a deterioration estimator and a shape-prior modulation block to automatically adjust the model’s contour-following ability. The deterioration estimator assesses the deterioration ratio that depicts the similarity of the provided masks to explicit masks. Features from the Stable Diffusion (SD) [Rombach *et al.*, 2022] encoders are utilized during the estimation, as SD effectively encodes the shape priors of different objects. Then, we modulate this shape prior to the zero-convolution layers of ControlNet through the proposed shape-prior modulation block. This design enables extra control over the strength of contour instructions and adapts the model to the guidance of inaccurate contours. As Fig. 1 shows, our method follows object position and poses guided by inexplicit masks, keeping high fidelity and spatial control over T2I generation.

This paper primarily focuses on ControlNet for two reasons. Firstly, ControlNet is the most representative and widely adopted method for spatially controllable T2I generation. It prevails over concurrent works for higher image quality and better preservation of outlines owing to the inherited powerful SD encoder and extensive training data. Secondly, ControlNet shares fundamental ideas and similar structures with existing adapter-based methods like T2I-Adapter [Mou *et al.*, 2023]. Moreover, these methods exhibit similar properties (*i.e.*, the contour-following ability) and face similar issues (*i.e.*, performance degradation with inaccurate contours). Examples are provided in Appendix. Therefore, our conclusions and methods can be potentially extended to these methods.

To summarize, our contributions are as follows:

- We study the contour-following ability of ControlNet quantitatively by examining its performance on masks of varying precision and hyperparameter settings. We reveal inexplicit masks would severely degrade image fidelity for strong priors induced by inaccurate contours.
- We propose a novel deterioration estimator and a shape-prior modulation block to integrate shape priors into ControlNet, namely Shape-aware ControlNet, which realizes robust interpretation of inexplicit masks.
- Our method adapts ControlNet to more flexible conditions like scribbles. We showcase its application scenarios like modifying object shapes and creative composition generation with masks of varying precision.

2 Related Works

Training with Spatial Signals An intuitive solution to introduce spatial control is training models with spatially aligned conditions from scratch. Make-A-Scene [Gafni *et al.*,

2022] employs scene tokens derived from dense segmentation maps during generation, enabling complex scene generation and editing. SpaText [Avrahami *et al.*, 2023] extends it to open-vocabulary scenarios and introduces spatio-textual representations for sparse scene control. Composer [Huang *et al.*, 2023] decomposes images to representative factors like edges and then trains a model to recompose the input from these factors. However, training models from scratch requires large-scale training data and high computational costs.

Adapters for Spatial Control. Another kind of work focuses on the utilization of adapters to inject spatial control into the pre-trained T2I models. For example, GLIGEN [Li *et al.*, 2023] involves gated self-attention layers to control the spatial layout during generation. T2I-adapter [Mou *et al.*, 2023] and ControlNet encode the spatial guidance via lightweight adapters or duplicated UNet structures, which are then fed into the decoder to control spatial structures like shapes and contours. Uni-ControlNet [Zhao *et al.*, 2023a], UniControl [Qin *et al.*, 2023], and Cocktail [Hu *et al.*, 2023] consolidate multi-modal conditions within a single framework. Since the base models are always frozen, these methods obtain better computational and data efficiency while retaining the generation ability of the base models. Despite these appealing characteristics, the impact of inexplicit masks is overlooked in these works, which may cause significant artifacts in generated images. Our proposed method can also be extended to these approaches to address this limitation.

3 Preliminary

ControlNet introduces a network to control T2I generation models, *i.e.*, Stable Diffusion (SD), with extra spatially localized, task-specific conditional images including Canny edges, Hough lines, fake scribbles, key points, segmentation masks, shape normals, depths, and so on. Given one encoder block $F(\cdot; \theta)$ of SD parameterized by θ , it accepts the input feature \mathbf{x} and output $\mathbf{y} = F(\mathbf{x}; \theta)$. ControlNet freezes the block and makes a trainable copy $F(\cdot; \theta')$ with parameter θ' to inject additional condition \mathbf{c} with zero convolution, formulated as,

$$\mathbf{y}_{\mathbf{c}} = F(\mathbf{x}; \theta) + \lambda * Z(F(\mathbf{x} + Z(\mathbf{c}; w_1); \theta'); w_2), \quad (1)$$

where $Z(\cdot; w_1)$ and $Z(\cdot; w_2)$ are two 1×1 zero convolution layers with parameters w_1, w_2 initialized with zeros for stable training. $\mathbf{y}_{\mathbf{c}}$ is the output feature modulated by spatial control signals. λ , namely *conditioning scale*, is introduced during inference to adjust condition strength. Since features are additive, it allows compositions of multiple conditions, also known as the Multi-ControlNet [Zhang *et al.*, 2023a].

Classifier-free Guidance (CFG) [Ho and Salimans, 2022] is a widely employed technique in generative diffusion models to increase image quality. Given a latent noise \mathbf{z} , CFG is conducted through mixing samples generated by an unconditional model $\epsilon_{\theta}(\cdot)$ and a jointly trained conditional model $\epsilon_{\theta}(\cdot, \mathbf{c})$, which is computed as,

$$\tilde{\epsilon}_{\theta}(\mathbf{z}, \mathbf{c}) = \epsilon_{\theta}(\mathbf{z}, \mathbf{c}) + \omega * (\epsilon_{\theta}(\mathbf{z}, \mathbf{c}) - \epsilon_{\theta}(\mathbf{z})), \quad (2)$$

where $\tilde{\epsilon}_{\theta}(\mathbf{z}, \mathbf{c})$ represents the final output under condition \mathbf{c} . ω is a scaling factor for a trade-off between image quality

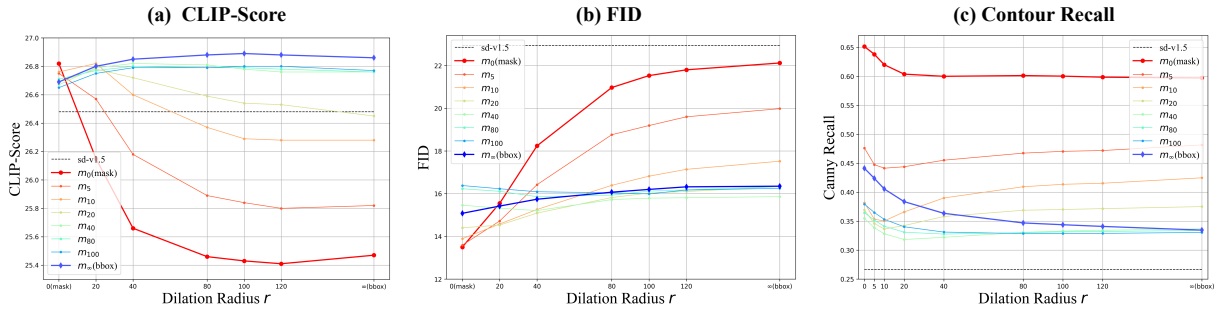


Figure 2: The metric curves of ControlNet- m_r on masks at varying levels of precision. The vanilla ControlNet, *i.e.*, ControlNet- m_0 , suffers from dramatic degradation on CLIP-Score and FID on deteriorated masks, but still keeps adhered to contours of provided masks.

and diversity, namely *CFG scale*. In this paper, spatial conditions are injected into both $\epsilon_\theta(\cdot)$ and $\epsilon_\theta(\cdot, c)$ when conducting classifier-free guidance with ControlNet.

4 Visiting Contour-following Ability

This section studies the contour-following ability from two aspects, including the performance on masks of varying precision and its interaction with hyperparameters, *i.e.*, CFG scale, conditioning scale, and condition injection strategy.

4.1 Setup

We utilize the most common real-world control signal, *i.e.*, object mask for experiments. The object mask is simple but effective in covering shape information. For simplicity, we focus on plain binary masks in experiments, which are the most straightforward signals in applications. This choice also helps to exclude the impacts of color and occlusion.

Datasets. Following [Zhang *et al.*, 2023b], our experiments involve COCO images [Lin *et al.*, 2014] and corresponding captions [Chen *et al.*, 2015]. We utilize instance masks from LVIS [Gupta *et al.*, 2019], which offers sparse and precise human-annotated object masks of COCO images with over 1200 object classes. We filter out images containing empty annotations, resulting in 114k image-caption-mask triplets for training and 4.7k for testing, namely COCO-LVIS.

Implementation Details. We adopt SD v1.5 [Runway, 2022] as the base model, and ControlNet is trained from scratch on COCO-LVIS for ten epochs with a learning rate of $1e-5$. We take 50% prompt dropping for classifier-free guidance while keeping the SD parameters frozen. We use UniPC [Zhao *et al.*, 2023b] sampler with 50 sampling steps. To evaluate, we take human-annotated masks for control and generate four images per caption. CFG scale and conditioning scale are set to 7.5 and 1.0 if there is no extra illustration.

Metrics. CLIP-Score (ViT-L/14) [Hessel *et al.*, 2021] and FID [Heusel *et al.*, 2017] are adopted as two basic metrics to measure text-image alignment and image fidelity. In addition, as ControlNet tends to preserve all contour structures provided in the conditional images, we calculate the number of edge pixels retained in the generated images, namely *Contour-Recall (CR)*, to measure the contour-following effects quantitatively. Supposing a conditional image c and

generated images $X = \{x_i\}_{i=1}^N$, CR is defined as the recall of edge pixels in the control inputs, formulated as,

$$CR = \frac{1}{N} \sum_{i=1}^N \frac{|MaxPool(D(x_i), \sigma) \cap (D(c))|}{|D(c)|}, \quad (3)$$

where $D(\cdot)$ is an edge detector that returns binary edge maps. $MaxPool(\cdot, \sigma)$ is a max-pooling function to tolerate an edge detection error of σ -pixels. In our implementation, we utilize the Canny edge detector and set a tolerance as $\sigma = 2$. Higher CR indicates stronger contour-following ability.

4.2 Impact of Inexplicit Masks

To clarify concerns about ControlNet’s performance on inexplicit masks, we first imitate inaccurate control signals by dilating object masks m with progressive radius $r (r \geq 0)$. The dilated mask is denoted as m_r , where m_0 presents masks with precise contours. Considering that bounding-box masks only convey object position and size without identifiable contours, we take an intersection over the dilated mask m_r and the bounding-box mask, denoted as b , to construct inexplicit masks of various precision, formulated as,

$$m_r = Dilate(m, r) \cap b, \quad (4)$$

where the bounding-box mask b can also be expressed as the extreme case $m_\infty (b \subset m_\infty)$. In the rest of the paper, we use m_∞ to denote the bounding-box mask.

We use the notation *ControlNet- m_r* to denote ControlNet trained with deteriorated masks m_r , where the vanilla ControlNet trained with precise masks is ControlNet- m_0 . We test these models on masks at varying deterioration degrees to explore the performance of ControlNet with inexplicit masks and its contour-following ability. Fig. 2 presents the experimental results. Here are two main observations.

➊ **The vanilla ControlNet, *i.e.*, ControlNet- m_0 , strictly adheres to the provided outlines, where inexplicit masks would cause severe performance degradation.** As shown in Fig. 1, the generated images are faithful to the contours of the control inputs under various control modalities, which is the key to excellent spatial controllable generation. One underlying reason is supposed to be that edges provide a shortcut to reconstruct input images. Therefore, ControlNet exhibits strong contour instructions during the generation process.

However, such a contour-following ability takes no account for inaccurate contours and maintains a high average CR of

	m_0	m_5	m_{10}	m_{20}	m_{40}
ControlNet - m_0	0.65	0.51	0.39	0.36	0.35
ControlNet - m_5	0.48	0.62	0.50	0.40	0.38
ControlNet - m_{10}	0.38	0.45	0.54	0.42	0.38
ControlNet - m_{20}	0.37	0.38	0.40	0.47	0.39
ControlNet - m_{40}	0.35	0.36	0.36	0.39	0.37

Figure 3: Illustration of the inductive bias of $ControlNet-m_r$ conditioned on m_r , where high CR on m_0 indicates models implicitly learned the dilation radius r .

over 60% in Fig. 2. While it allows minor editing by manipulating masks to some extent, this property imposes severe problems on image realism when inaccurate contours are provided. Similar observations are also noted in [Voynov *et al.*, 2023; Bhat *et al.*, 2023; Singh *et al.*, 2023]. For example, ControlNet tends to interpret rectangle masks as boards rather than animals specified in the prompt, causing incorrect spatial layouts and distorted objects. It is also reflected in a degradation of 1.35 CLIP-score and 8.62 FID. Thus, precise masks with accurate contours are necessary for high-quality generation. However, obtaining masks with accurate contours is challenging, especially for non-expert users.

② **Training ControlNet with deteriorated masks also converges and exhibits higher robustness on masks of varying precision with a sacrifice of contour instructions.** We further train a series of ControlNet on manually deteriorated masks. Surprisingly, we find ControlNet converges successfully with all conditions, even on the extreme bounding-box masks. As illustrated in Fig. 2, training with deteriorated masks consistently improves ControlNet’s robustness in interpreting inexplicit masks with better CLIP-score and FID at the cost of weak contour-following ability.

However, ControlNet trained with dilated masks implicitly assumes the presence of dilation in the provided mask, even for precise masks. Fig. 3 reports the CR referring to precise mask m_0 when ControlNet- m_r is conditioned on dilated masks m_r . As ControlNet- m_r keeps a CR on m_0 over 0.5 until $r > 20$, suggesting that models infer and follow precise contours based on the provided m_r . Examples are provided in the Appendix. This effect diminishes as the radius r increases, and ControlNet- m_r ($r \geq 40$) shows weak contour-following ability and prompts object positions via masks.

Moreover, training ControlNet with severely deteriorated masks, *e.g.*, bounding-box masks, yields poorer CLIP-score and FID with precise masks as shown in Fig. 2. Examples in Fig. 7 illustrate that ControlNet- m_∞ probably misinterprets one whole object mask as multiple small objects. This reminds us that too weak contour instructions can also cause problematic images and deviate from user intentions. So, it is worthwhile to develop a method to make contour-following ability more controllable, thereby fulfilling robust interpretation with inexplicit masks of varying precision.

4.3 Impact of Hyperparameters

As a common practice, adjusting hyperparameters like CFG scales is useful to achieve satisfactory generation results.

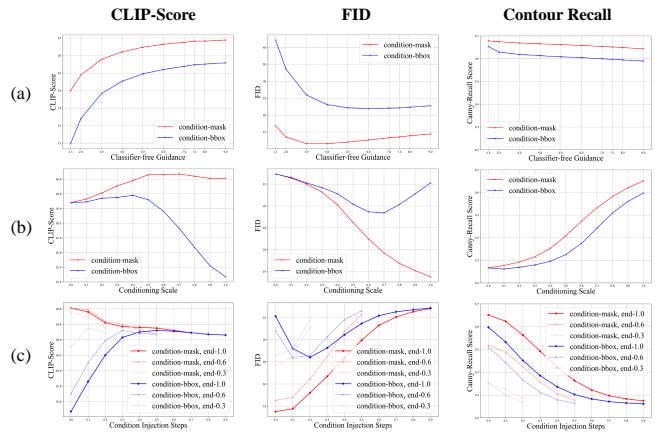


Figure 4: Metric curves of (a) CFG scale, (b) conditioning scale, and (c) condition injection strategy. Red denotes the performance on the precise mask m_0 , and blue denotes the bounding-box mask m_∞ .

Therefore, we investigate how hyperparameters impact the contour-following ability and reveal several guidelines.

Specifically, we test the vanilla ControlNet (ControlNet- m_0), under two extreme condition cases, *i.e.*, precise mask m_0 and bounding-box mask m_∞ . Three core hyperparameters are considered, *i.e.*, CFG scale λ , conditioning scale ω , and condition injection strategy. Quantitative results are revealed in Fig. 4. Examples are presented in the Appendix.

Effects of Classifier-free Guidance ω . Under both conditions, ControlNet maintains high CR scores under all CFG scales, showing little impact on contour-following ability. This is because conditioning signals are added to both $\epsilon_\theta(\cdot)$ and $\epsilon_\theta(\cdot, c)$ in Eq. 2. Moreover, performance on precise mask m_0 always surpasses that on m_∞ , indicating precise control inputs improve image quality. The trends of CLIP-Score and FID curves align with common sense, where a relatively higher ω brings better fidelity and text faithfulness.

Effects of Conditioning Scale λ . The conditioning scale decides the strength of control signals as Eq.1. A higher λ imposes stronger instructions, consistent with increasing CR scores under both conditions. However, the behavior diverges on CLIP-Score and FID when increasing λ . While both CLIP-Score and FID almost consistently increase on m_0 , its performance on m_∞ increases slightly at the very beginning but then declines dramatically, showing a large performance gap with m_0 . This reveals a trade-off between image quality and spatial control with bounding-box masks, where $\lambda \in [0.5, 0.7]$ are recommended. Finding suitable λ for masks of varying precision usually requires tens of attempts.

Effects of Condition Injection Strategy. We divide the sampling steps into ten stages during the reverse sampling phase for experiments. As shown in Fig. 4(c), all stages contribute to contour instructions during the generation process under both conditions. The first 10% \sim 40% steps hold the key, consistent with observations in [Mou *et al.*, 2023]. In addition, a similar divergence of CLIP-Score and FID curves is observed between the two conditions, further declaring the performance gap between explicit and inexplicit masks.

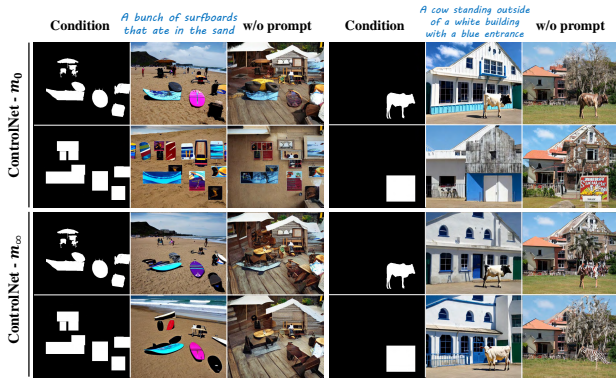


Figure 5: Illustrations on the difference between explicit and inexplicit masks for control. The contour-following ability induces strong priors from contours, causing conflicts with textual prompts.

In summary, while the CFG scale has little impact on the contour-following ability, smaller conditioning scales and discarding conditions at early reverse sampling stages help to relieve contour instructions. This strategy helps to improve image fidelity and text faithfulness for inexplicit masks. However, subtle changes to such hyperparameters may lead to dramatic changes in image appearance (see Appendix). Hence, it is tricky to search for the ideal combination of hyperparameters for each image, and it takes risks of violating spatial control for a trade-off.

4.4 Empirical Analysis

To clarify the difference between explicit and inexplicit mask controls, we conduct comparisons between ControlNet- m_0 and ControlNet- m_∞ on precise masks m_0 and bounding-box masks m_∞ in Fig. 5. By removing textual prompts, we find that the strong contour-following ability of vanilla ControlNet derives intense shape priors from contours, thus it infers specific objects from the mask. As inexplicit masks introduce incorrect shape priors, they result in conflicts with textual prompts or violation of spatial control. For example, bounding-box masks are misinterpreted as the door in Fig. 5. This is why vanilla ControlNet fails to interpret inaccurate contours with correct content. VisorGPT [Xie *et al.*, 2023] also validates that conditional generative models implicitly learn visual priors from the data, such as size and shape. If spatial conditions deviate from that prior, it would lead to artifacts and incorrect contents. In contrast, ControlNet- m_∞ relies less on the shape priors from the conditional mask but prompts object locations for spatial control. This leads to improved text alignment and robustness on inexplicit masks. However, ControlNet- m_∞ exhibits weak control with precise masks. So, it is necessary to develop a method to adapt ControlNet to masks of varying precision.

5 Shape-aware ControlNet

To enhance ControlNet’s ability to interpret inexplicit masks robustly instead of blindly adhering to contours, we introduce a novel deterioration estimator and a shape-prior modulation block, namely Shape-aware ControlNet, as depicted in Fig. 6.

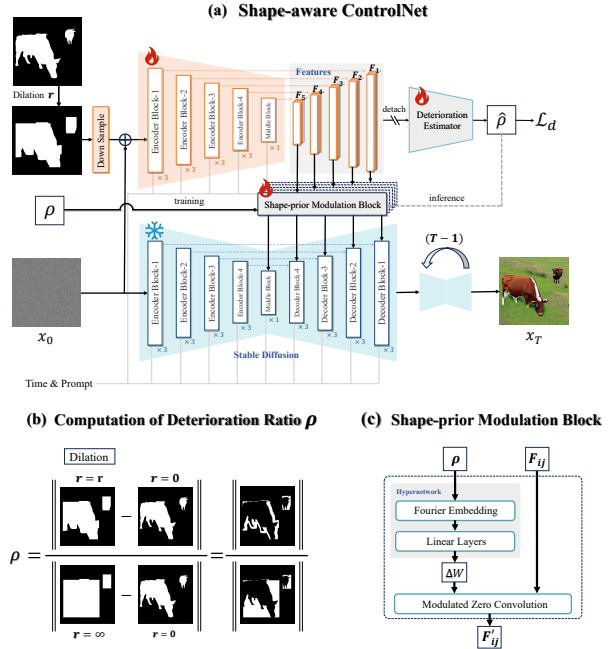


Figure 6: The overall architecture of Shape-aware ControlNet. It contains 1) a deterioration estimator to assess the deterioration ratio of inexplicit masks, and 2) a shape-prior modulation block to modulate this ratio to ControlNet to adjust the contour-following ability for robust spatial control with inexplicit masks.

5.1 Deterioration Estimator

We first introduce the deterioration ratio ρ , which depicts the gap between the inexplicit masks and explicit shape priors of specific objects, formulated as,

$$\rho = \frac{|S(m_r) - S(m_0)|}{|S(m_\infty) - S(m_0)|}, \quad (5)$$

where $S(\cdot)$ returns the area of masks, and $\rho \in [0, 1]$. Eq. 5 measures the shape priors of masks, where $\rho = 0$ indicates the exact object shape and $\rho = 1$ means no identifiable shape.

While computing the deterioration ratio ρ based on precise object masks is straightforward, estimating ρ from inexplicit masks is non-trivial. This motivates us to train an extra deterioration estimator. Since ControlNet- m_r can imply the dilation radius r (refer to § 4.2), we suppose ControlNet implicitly learns shape priors from deteriorated masks. So, we construct a deterioration estimator with stacked convolutional and linear layers with batch normalization, to predict the ratio from encoder features $\{F_{ij}\}$, where F_{ij} denotes the j -th feature from the i -th encoder block. Such a design proves to provide accurate estimation as discussed in § 6.3. We train the estimator separately with an L_2 loss and detach the gradients from the encoder to avoid negative effects on the convergence of ControlNet.

5.2 Shape-prior Modulation Block

Taking the shape prior ρ as an extra condition, we design a shape-prior modulation block inspired by [Karras *et al.*, 2019]. Specifically, we encode ρ into Fourier embedding.

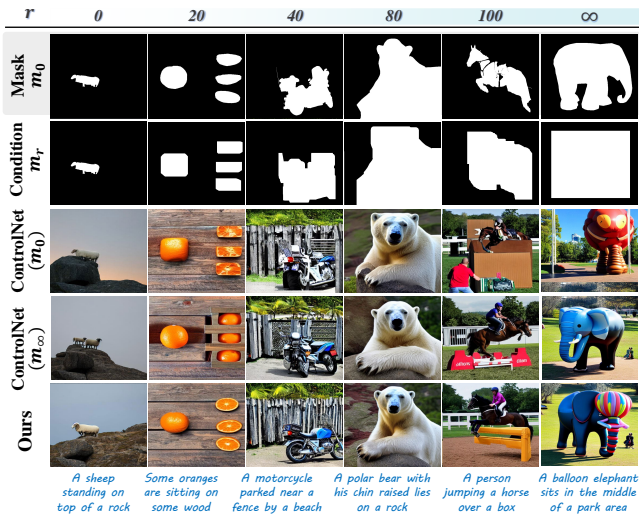


Figure 7: Visualized comparison between the vanilla ControlNet and Shape-aware ControlNet with masks at varying levels of precision.

Then, we employ a hypernetwork [Ha *et al.*, 2016] to modulate shape priors to zero convolution layers in ControlNet as illustrated in Fig. 6(c). Supposing a zero convolution $Z(\cdot; w)$ parameterized by w and ControlNet encoder feature F_{ij} , the modulated feature F'_{ij} is computed as,

$$F'_{ij} = Z(F_{ij}; (1 + \Delta W) \cdot w), \quad (6)$$

where $\Delta W = H(\rho)$, and $H(\cdot)$ is a hypernetwork constructed by multiple linear layers.

6 Experiments

6.1 Implementation Details

The baselines including ControlNet- m_0 and ControlNet- m_∞ are implemented as § 4.1. We inherit the same setting to train our shape-prior modulation block on COCO-LVIS for 10 epochs from scratch with a learning rate of $1e - 5$, where the dilation radius is uniformly sampled from 0 to 80. The deterioration estimator is trained for another 10 epochs individually with gradient-detached features from ControlNet.

Metrics We employ CLIP-Score and FID for evaluation. As CR metric would fail when the strict alignment of contours is violated, we propose two additional metrics inspired by [Hinz *et al.*, 2020], namely Layout Consistency (LC) and Semantic Retrieval (SR). Definitions are as follows.

Definition 1 (Layout Consistency, LC). *LC measures the spatial alignment between conditional masks and generated images. Supposing detected bounding boxes $\{a_i\}_{i=1}^M$ and those of control masks $\{b_j\}_{j=1}^N$, LC is computed as follows:*

$$LC = \frac{|\bigcup_i^M a_i \cap \bigcup_j^N b_j|}{|\bigcup_i^M a_i \cup \bigcup_j^N b_j|}. \quad (7)$$

Definition 2 (Semantic Retrieval, SR). *SR is a retrieval measurement to verify whether the semantic objects assigned in*

Metric	Method	r						AVG
		0	20	40	80	100	∞	
CLIP-Score	ControlNet- m_0	26.82	26.15	25.66	25.46	25.43	25.47	25.83
	ControlNet- m_∞	26.69	26.80	26.85	26.88	26.89	26.86	26.83
	Ours	26.88	26.87	26.89	26.89	26.87	26.83	26.87
FID	ControlNet- m_0	13.50	15.55	18.24	20.97	21.53	22.12	18.65
	ControlNet- m_∞	15.08	15.42	15.74	16.07	16.20	16.35	15.81
	Ours	13.20	13.62	14.07	14.72	14.78	15.12	14.25
LC	ControlNet- m_0	0.605	0.531	0.489	0.469	0.466	0.465	0.504
	ControlNet- m_∞	0.534	0.551	0.555	0.555	0.555	0.553	0.551
	Ours	0.601	0.586	0.577	0.569	0.567	0.561	0.577
SR	ControlNet- m_0	0.522	0.440	0.374	0.327	0.320	0.303	0.381
	ControlNet- m_∞	0.401	0.430	0.438	0.444	0.445	0.446	0.434
	Ours	0.513	0.503	0.495	0.482	0.477	0.462	0.489

Table 1: Performance comparison of our method and baselines, *i.e.*, the vanilla ControlNet (ControlNet- m_0) and ControlNet- m_∞ trained with bounding-box masks under different dilation radius r .

the prompt are generated. Supposing M detected object categories $S = \{s_i\}_{i=1}^M$ over confidence threshold t and N assigned labels $L = \{l_j\}_{j=1}^N$, SR is formulated as,

$$SR = \frac{|S \cap L|}{|L|}. \quad (8)$$

Specifically, we utilize an open-vocabulary object detector, *i.e.*, OWL-ViT [Matthias Minderer, 2022] following VISOR [Gokhale *et al.*, 2022]. We set the confidence threshold $t = 0.1$ and use instance labels as prompts.

6.2 Comparisons with Vanilla ControlNet

As Tab. 1 depicts, our method achieves competitive or better performance on all metrics, demonstrating robustness under all dilation radius. Visualized results in Fig. 7 further illustrate the effectiveness of our method. ControlNet- m_0 tends to blindly follow the outlines of control inputs, thus suffering from unnatural images or violation of user intentions, especially when it is conditioned on largely deteriorated masks. On the other hand, ControlNet- m_∞ struggles with precise masks with fine details like misinterpreting a single instance mask into multiple objects. In contrast, our method excels in understanding object orientations and shapes according to in-explicit masks, thanks to additional guidance of shape priors. More examples are available in the Appendix.

6.3 Ablation Studies

Comparison with random dilation augmentation. As augmentation with random dilated masks serves as an intuitive and straightforward solution to improve the robustness of deteriorated masks, we compare this strategy with our Shape-aware ControlNet in Tab. 2. While this data augmentation strategy is also effective, our method achieves consis-

Method	CLIP \uparrow	FID \downarrow	LC \uparrow (%)	SR \uparrow (%)
ControlNet- m_0	25.83	18.65	0.504	0.381
+ Random Aug	26.76	15.28	0.565	0.475
Ours	26.87	14.25	0.577	0.489

Table 2: Comparison with random dilation for augmentation.

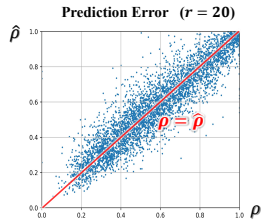


Figure 8: The error of deterioration estimator when radius $r = 20$.

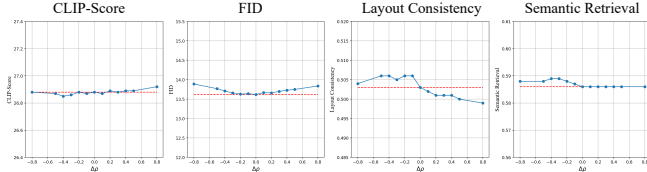


Figure 9: The variation of metrics under $(\rho + \Delta\rho)$ when $r = 20$.

tently higher performance on all metrics. Moreover, we highlight that our method provides users with the convenience of easily modifying the shape of generated objects through additional control over shape priors.

Accuracy of deterioration estimator. We validate the accuracy of our proposed deterioration estimator in Fig. 8. The overall average $L1$ error is 5.47%. Owing to the robustness of the modulation block, such an error shows minimal impact on the fidelity of generated images as validated in Tab. 3. Detailed error curves are presented in the Appendix.

Robustness on shape priors. We further examine the robustness of our method on different shape priors. We take dilation radius $r = 20$ and manually adjust the shape prior ρ to $(\rho + \Delta\rho) \in [0, 1]$, where $\Delta\rho \in [0, 1]$. As shown in Fig. 9, changing ρ reveals little impact on the text faithfulness and image quality. But lower ρ encourages better adherence to conditional masks, resulting in slightly higher LC with the assigned control masks, and vice versa. Visualized examples of tuning ρ can be found in Fig. 11.

6.4 Applications

We showcase several applications of our method. For page limitations, additional examples are included in Appendix.

Generation with TikZ sketches and scribbles. Since our Shape-aware ControlNet interprets inexplicit masks robustly, we observe its effectiveness in handling programmatic sketches and human scribbles as shown in Fig. 10. Our method generates reasonable images with abstract or inexplicit masks while keeping high fidelity and spatial control. We follow [Zhang *et al.*, 2023b] to prompt GPT-4 to produce TikZ codes for object sketches. Human scribbles are converted from Sketchy [Sangkloy *et al.*, 2016].

Ratio	CLIP \uparrow	FID \downarrow	LC \uparrow (%)	SR \uparrow (%)
ρ	26.88	14.21	0.576	0.489
$\hat{\rho}$	26.87	14.25	0.577	0.489

Table 3: Performance comparison between ρ and predicted $\hat{\rho}$.

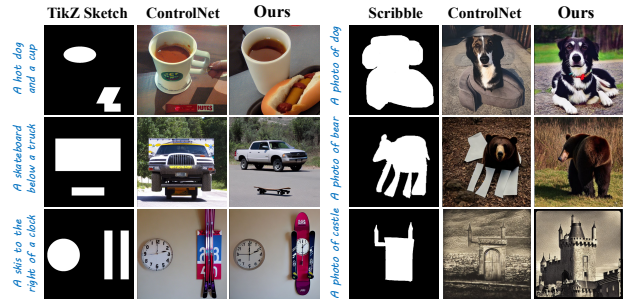


Figure 10: Performance comparison on TikZ sketches and scribbles.

Shape-prior modification. While the deterioration estimator provides the deterioration ratio $\hat{\rho}$ for reference, we can manually set ρ to control the shape prior. It determines how much the generated objects conform to the provided conditional masks as shown in Fig. 11. We notice it is possible to extend $\hat{\rho}$ to values other values, even though $\rho \in [0, 1]$ for training. A lower $|\rho|$ encourages stronger adherence to the contours of the provided masks.

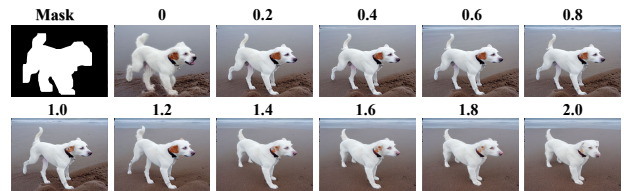


Figure 11: Shape-prior control via deterioration ratio ρ .

Composable shape-controllable generation. We realize composable shape control via a multi-ControlNet structure [Zhang *et al.*, 2023a], where we generate images by assigning different priors to each part of control masks. This enables strict shape control over specifically assigned masks while allowing T2I diffusion models to unleash creativity in imagining objects of diverse shapes within inexplicit masks. A vivid example is presented in Fig. 12, where the parrots share fixed contours but hats are generated within masked areas in various styles, and vice versa.

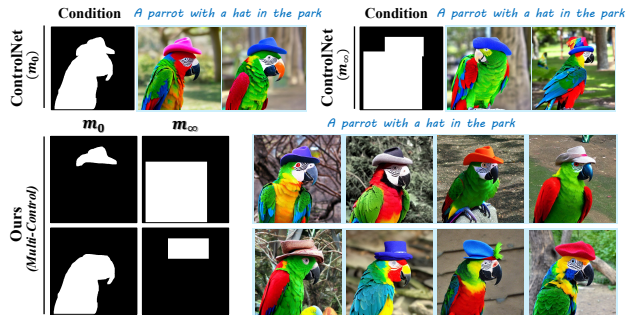


Figure 12: Examples of composable generation with explicit and inexplicit masks, showing flexible control with diverse results.

7 Conclusion

In this paper, we reveal insights into the core traits of ControlNet, *i.e.*, the contour-following ability. We quantitatively validate this property by distorting conditional masks and tuning hyper-parameters, where we uncover severe performance degradation caused by inexplicit masks. In light of this, we propose a novel deterioration estimator and a shape-prior modulation block to endow ControlNet with shape-awareness to robustly interpret inexplicit masks with an extra shape-prior control. This exhibits the potential of employing ControlNet in more creative scenarios like user scribbles.

References

- [Avrahami *et al.*, 2023] Omri Avrahami, Thomas Hayes, Oran Gafni, Sonal Gupta, Yaniv Taigman, Devi Parikh, Dani Lischinski, Ohad Fried, and Xi Yin. Spatext: Spatio-textual representation for controllable image generation. In *Proceedings of the IEEE/CVF Conference on Computer Vision and Pattern Recognition*, pages 18370–18380, 2023.
- [Bhat *et al.*, 2023] Shariq Farooq Bhat, Niloy J Mitra, and Peter Wonka. Loosecontrol: Lifting controlnet for generalized depth conditioning. *arXiv preprint arXiv:2312.03079*, 2023.
- [Chen *et al.*, 2015] Xinlei Chen, Hao Fang, Tsung-Yi Lin, Ramakrishna Vedantam, Saurabh Gupta, Piotr Dollár, and C Lawrence Zitnick. Microsoft coco captions: Data collection and evaluation server. *arXiv preprint arXiv:1504.00325*, 2015.
- [Gafni *et al.*, 2022] Oran Gafni, Adam Polyak, Oron Ashual, Shelly Sheynin, Devi Parikh, and Yaniv Taigman. Make-a-scene: Scene-based text-to-image generation with human priors. In *European Conference on Computer Vision*, pages 89–106. Springer, 2022.
- [Gokhale *et al.*, 2022] Tejas Gokhale, Hamid Palangi, Bismira Nushi, Vibhav Vineet, Eric Horvitz, Ece Kamar, Chitta Baral, and Yezhou Yang. Benchmarking spatial relationships in text-to-image generation. *arXiv preprint arXiv:2212.10015*, 2022.
- [Gupta *et al.*, 2019] Agrim Gupta, Piotr Dollar, and Ross Girshick. Lvis: A dataset for large vocabulary instance segmentation. In *Proceedings of the IEEE/CVF conference on computer vision and pattern recognition*, pages 5356–5364, 2019.
- [Ha *et al.*, 2016] David Ha, Andrew Dai, and Quoc V. Le. Hypernetworks, 2016.
- [Hessel *et al.*, 2021] Jack Hessel, Ari Holtzman, Maxwell Forbes, Ronan Le Bras, and Yejin Choi. Clipscore: A reference-free evaluation metric for image captioning. *arXiv preprint arXiv:2104.08718*, 2021.
- [Heusel *et al.*, 2017] Martin Heusel, Hubert Ramsauer, Thomas Unterthiner, Bernhard Nessler, and Sepp Hochreiter. Gans trained by a two time-scale update rule converge to a local nash equilibrium. *Advances in neural information processing systems*, 30, 2017.
- [Hinz *et al.*, 2020] Tobias Hinz, Stefan Heinrich, and Stefan Wermter. Semantic object accuracy for generative text-to-image synthesis. *IEEE transactions on pattern analysis and machine intelligence*, 44(3):1552–1565, 2020.
- [Ho and Salimans, 2022] Jonathan Ho and Tim Salimans. Classifier-free diffusion guidance. *arXiv preprint arXiv:2207.12598*, 2022.
- [Hu *et al.*, 2023] Minghui Hu, Jianbin Zheng, Daqing Liu, Chuanxia Zheng, Chaoyue Wang, Dacheng Tao, and Tat-Jen Cham. Cocktail: Mixing multi-modality controls for text-conditional image generation. *arXiv preprint arXiv:2306.00964*, 2023.
- [Huang *et al.*, 2023] Lianghua Huang, Di Chen, Yu Liu, Yujun Shen, Deli Zhao, and Jingren Zhou. Composer: Creative and controllable image synthesis with composable conditions. *arXiv preprint arXiv:2302.09778*, 2023.
- [Karras *et al.*, 2019] Tero Karras, Samuli Laine, and Timo Aila. A style-based generator architecture for generative adversarial networks. In *Proceedings of the IEEE/CVF conference on computer vision and pattern recognition*, pages 4401–4410, 2019.
- [Li *et al.*, 2023] Yuheng Li, Haotian Liu, Qingyang Wu, Fangzhou Mu, Jianwei Yang, Jianfeng Gao, Chunyuan Li, and Yong Jae Lee. Gligen: Open-set grounded text-to-image generation. In *Proceedings of the IEEE/CVF Conference on Computer Vision and Pattern Recognition*, pages 22511–22521, 2023.
- [Lin *et al.*, 2014] Tsung-Yi Lin, Michael Maire, Serge Belongie, James Hays, Pietro Perona, Deva Ramanan, Piotr Dollár, and C Lawrence Zitnick. Microsoft coco: Common objects in context. In *Computer Vision—ECCV 2014: 13th European Conference, Zurich, Switzerland, September 6–12, 2014, Proceedings, Part V 13*, pages 740–755. Springer, 2014.
- [Matthias Minderer, 2022] et.al. Matthias Minderer. Simple open-vocabulary object detection with vision transformers. *ECCV*, 2022.
- [Mou *et al.*, 2023] Chong Mou, Xintao Wang, Liangbin Xie, Jian Zhang, Zhongang Qi, Ying Shan, and Xiaoju Qie. T2i-adapter: Learning adapters to dig out more controllable ability for text-to-image diffusion models. *arXiv preprint arXiv:2302.08453*, 2023.
- [Qin *et al.*, 2023] Can Qin, Shu Zhang, Ning Yu, Yihao Feng, Xinyi Yang, Yingbo Zhou, Huan Wang, Juan Carlos Niebles, Caiming Xiong, Silvio Savarese, et al. Uni-control: A unified diffusion model for controllable visual generation in the wild. *arXiv preprint arXiv:2305.11147*, 2023.
- [Ramesh *et al.*, 2021] Aditya Ramesh, Mikhail Pavlov, Gabriel Goh, Scott Gray, Chelsea Voss, Alec Radford, Mark Chen, and Ilya Sutskever. Zero-shot text-to-image generation. In *International Conference on Machine Learning*, pages 8821–8831. PMLR, 2021.
- [Ramesh *et al.*, 2022] Aditya Ramesh, Prafulla Dhariwal, Alex Nichol, Casey Chu, and Mark Chen. Hierarchical

text-conditional image generation with clip latents. *arXiv preprint arXiv:2204.06125*, 1(2):3, 2022.

[Rombach *et al.*, 2022] Robin Rombach, Andreas Blattmann, Dominik Lorenz, Patrick Esser, and Björn Ommer. High-resolution image synthesis with latent diffusion models. In *Proceedings of the IEEE/CVF conference on computer vision and pattern recognition*, pages 10684–10695, 2022.

[Runway, 2022] Runway. Stable Diffusion v1-5, 2022.

[Saharia *et al.*, 2022] Chitwan Saharia, William Chan, Saurabh Saxena, Lala Li, Jay Whang, Emily L Denton, Kamyar Ghasemipour, Raphael Gontijo Lopes, Burcu Karagol Ayan, Tim Salimans, et al. Photorealistic text-to-image diffusion models with deep language understanding. *Advances in Neural Information Processing Systems*, 35:36479–36494, 2022.

[Sangkloy *et al.*, 2016] Patsorn Sangkloy, Nathan Burnell, Cusuh Ham, and James Hays. The sketchy database: learning to retrieve badly drawn bunnies. *ACM Transactions on Graphics (TOG)*, 35(4):1–12, 2016.

[Singh *et al.*, 2023] Jaskirat Singh, Jianming Zhang, Qing Liu, Cameron Smith, Zhe Lin, and Liang Zheng. Smart-mask: Context aware high-fidelity mask generation for fine-grained object insertion and layout control. *arXiv preprint arXiv:2312.05039*, 2023.

[Voynov *et al.*, 2023] Andrey Voynov, Kfir Aberman, and Daniel Cohen-Or. Sketch-guided text-to-image diffusion models. In *ACM SIGGRAPH 2023 Conference Proceedings*, pages 1–11, 2023.

[Xie *et al.*, 2023] Jinheng Xie, Kai Ye, Yudong Li, Yuexiang Li, Kevin Qinghong Lin, Yefeng Zheng, Linlin Shen, and Mike Zheng Shou. Learning visual prior via generative pre-training. In *Thirty-seventh Conference on Neural Information Processing Systems, 2023*.

[Zhang *et al.*, 2023a] Lvmin Zhang, Anyi Rao, and Maneesh Agrawala. Adding conditional control to text-to-image diffusion models. In *Proceedings of the IEEE/CVF International Conference on Computer Vision*, pages 3836–3847, 2023.

[Zhang *et al.*, 2023b] Tianjun Zhang, Yi Zhang, Vibhav Vineet, Neel Joshi, and Xin Wang. Controllable text-to-image generation with gpt-4. *arXiv preprint arXiv:2305.18583*, 2023.

[Zhao *et al.*, 2023a] Shihao Zhao, Dongdong Chen, Yen-Chun Chen, Jianmin Bao, Shaozhe Hao, Lu Yuan, and Kwan-Yee K Wong. Uni-controlnet: All-in-one control to text-to-image diffusion models. *arXiv preprint arXiv:2305.16322*, 2023.

[Zhao *et al.*, 2023b] Wenliang Zhao, Lujia Bai, Yongming Rao, Jie Zhou, and Jiwen Lu. Unipc: A unified predictor-corrector framework for fast sampling of diffusion models. *NeurIPS*, 2023.

Appendix

This appendix is organized as follows:

- Additional visualized examples with detailed illustrations are presented to supplement the main paper. (§A)
- We give a brief discussion about future works. (§B).

A Additional Qualitative Examples

We provide additional qualitative results to supplement the main paper. Tab. 4 gives a quick overview of all figures presented in Appendix and indicates where they are referenced in the main paper for supplementary. Details are as follows.

Fig ID	Reference (main paper)	Brief Illustration
Fig.13	§1, Line 100	More examples of ControlNet and T2I-adapter to illustrate their contour-following ability.
Fig.14	§4.2, Line 279	Visualization of the inductive bias of dilation radius r .
Fig.15	§4.3, Line 302, 339	Visual results for tuning hyperparameters.
Fig.16	§6.2, Line 443	More comparison examples of our method and ControlNet.
Fig.17	§6.3, Line 460	Error analysis for the deterioration estimator.
Fig.18	§6.4, Line 472	Generation with TikZ sketches.
Fig.19	§6.4, Line 472	Generation with user scribbles.
Fig.20	§6.4, Line 472	Examples for modifying shape priors.
Fig.21	§6.4, Line 472	Examples for composable shape-controllable generation.

Table 4: Quick overview of the figures in this Appendix.

Implication of dilation radius r . We further visualize examples of ControlNet- m_r with conditional masks of varying precision in Fig. 14. Note that ControlNet- m_r is trained with dilated masks m_r . As depicted in Fig. 14, ControlNet- m_r implicitly assumes the presence of dilation in the provided masks, even for precise masks. For instance, the zebra generated by ControlNet- m_r with conditional mask m_r (in red boxes) shares similar size and shape with the precise mask m_0 , which explains the high CR scores in Fig.3 in our main paper. In contrast, our Shape-aware ControlNet robustly interprets all deteriorated conditions thanks to additional control over the shape priors.

Visualized examples of tuning hyperparameters. Fig. 15 presents visualized results of the vanilla ControlNet under different hyperparameter settings, including the CFG scale ω , conditioning scale λ , and condition injection strategy in our main paper. The CFG scale ω exhibits minimal impact on the contour-following effect but enhances image fidelity with higher saturation. Lowering the conditioning scale λ and omitting conditions in the reverse sampling stages alleviate the strong contour instructions. However, because of the significant performance gaps between explicit and implicit conditions, bridging this gap and obtaining satisfactory

results solely through hyperparameter tuning is challenging. Moreover, sudden appearance changes usually occur when we adjust hyperparameters, making it tricky to find the optimal setting. Therefore, it is necessary to develop a method to robustly interpret inexplicit masks.

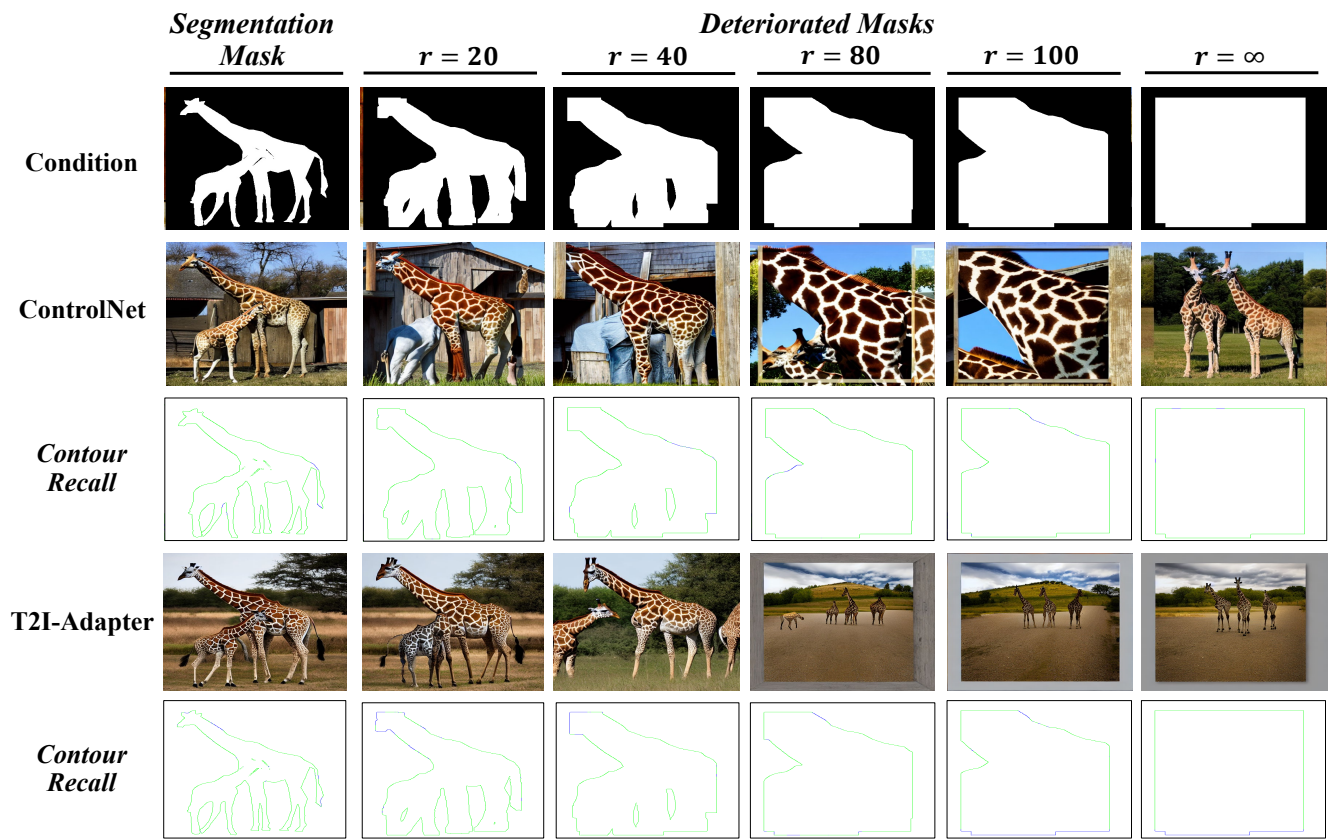
More visualized comparison with the vanilla ControlNet. In Fig. 16, we provide more examples of our Shape-aware ControlNet compared with the vanilla ControlNet. Our method not only achieves competitive results with ControlNet on precise masks, but also demonstrates an enhanced capability to interpret object shape and pose from inexplicit masks of varying precision.

Full results of error analysis for the deterioration estimator. Fig. 17 reports the full results of the estimation error for the proposed deterioration estimator. The overall averaged $L1$ error under different dilation radius r is 5.47%. We confirm that this error has little impact on the performance due to the robustness of the shape-prior modulation block, as discussed in the main paper §6.3.

More application examples. We showcase additional examples of our method in three application scenarios, including robust generation with TikZ sketches (Fig. 18) following [Zhang *et al.*, 2023b], human scribbles (Fig. 19) converted from Sketchy [Sangkloy *et al.*, 2016], modification of shape priors (Fig. 20), and composable shape-controllable generation (Fig. 21). These examples verify that our method helps extend ControlNet to creative applications with more flexible control signals, owing to controllable shape priors.

B Future Works

By far, we have demonstrated the effectiveness of our method in improving ControlNet in dealing with inexplicit masks, which is an essential topic in applying ControlNet in practical usage. Moreover, we have noted that the dramatic performance degradation caused by inexplicit masks is a common issue among methods that inject spatially aligned control signals for spatially controllable T2I generation. The results of T2I-Adapter [Mou *et al.*, 2023] are shown in Fig. 13, where large deterioration in the control masks would pose challenges in correctly understanding the spatial control signals. Since our method takes no assumption about the network that injects control signals into the generation process, it has the potential to extend to other adapter-based methods like T2I-Adapter to avoid deviation of spatial control brought by inexplicit masks. We leave this as our future work.

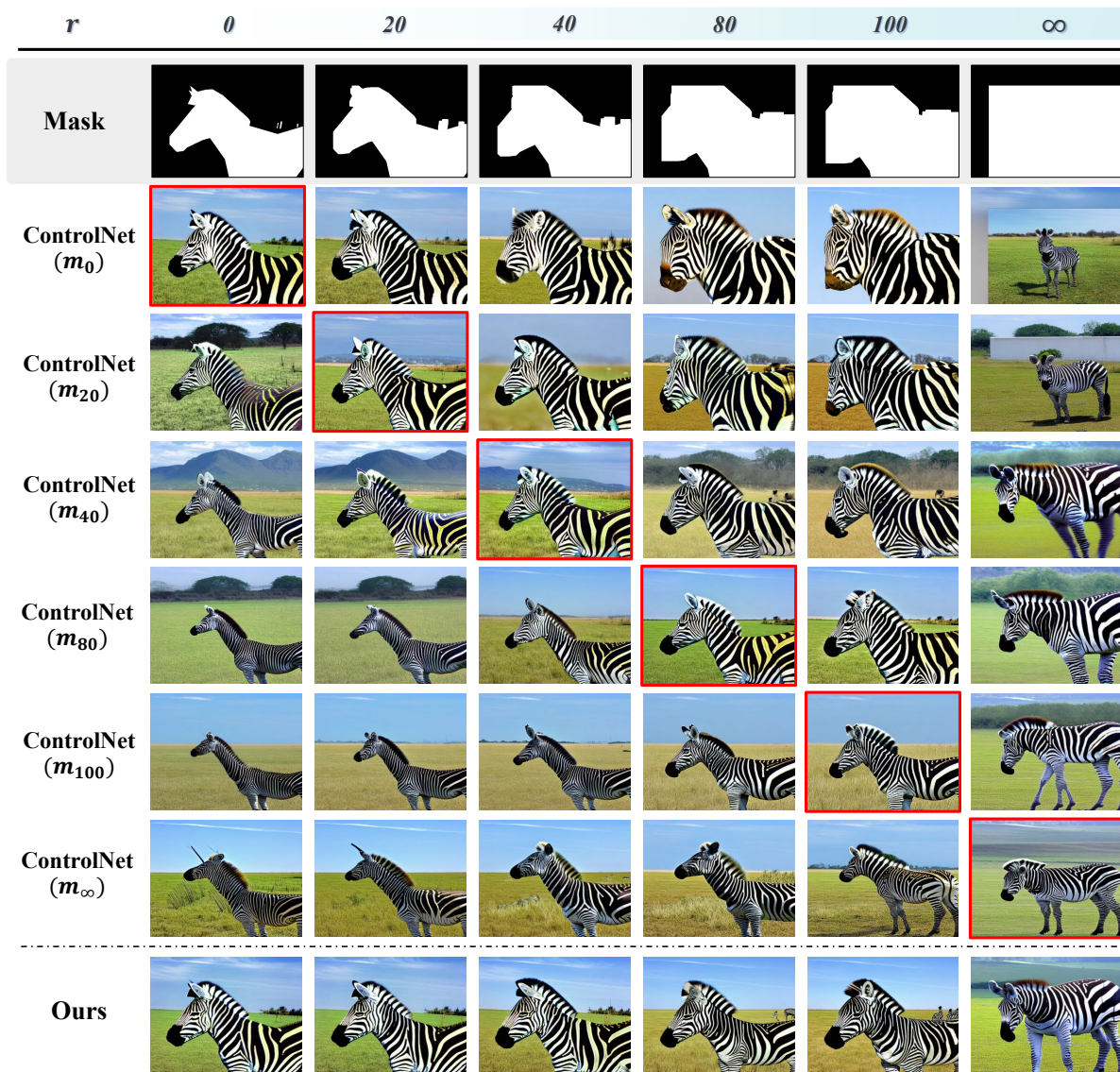


Prompt: Two giraffes are standing together outside a barn



Prompt: A zebra all by itself in the green forest

Figure 13: More examples of ControlNet and T2I-adapter illustrating spatially controllable generation with masks of varying precision. Both methods exhibit strong preservation of contours during the generation process. **Green** denotes the recalled contours and **blue** denotes the missing ones. Moreover, inexplicit masks with inaccurate contours would cause severe degradation of image fidelity and realism.



Prompt: *A zebra standing on top of a grass covered field*

Figure 14: Visualized examples to illustrate the inductive bias, where ControlNet- m_r implicitly learns the dilated radius r from the data. Therefore, it always assumes a dilation in the provided mask. The ControlNet- m_r conditioned on m_r (in red boxes) produces objects with similar shapes and sizes of mask m_0 . While ControlNet- m_{∞} also breaks the inductive bias, our method surpasses it in terms of image fidelity and additional control over the shape priors.

A sheep standing in a dry grass field

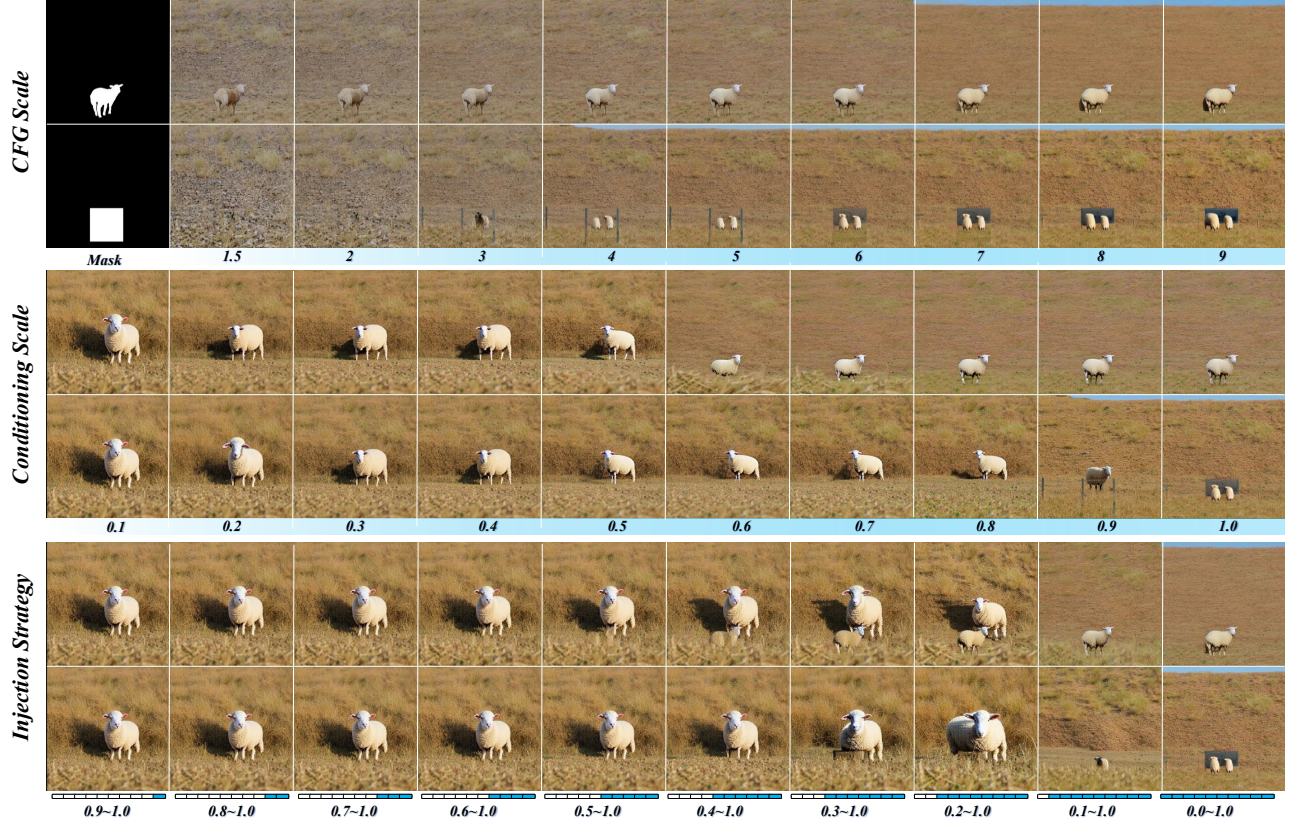


Figure 15: Visualized examples under different hyperparameter settings, *i.e.*, CFG scale, conditioning scale, and condition injection strategy. Though the CFG scale shows little impact on the contour-following ability, reducing conditioning scales and discarding conditions at early reverse sampling stages help to relieve contour instructions, resulting in better results with inexplicit conditional masks. However, it can be tricky and hard to achieve satisfactory results through hyperparameter tuning, especially for deteriorated control masks.

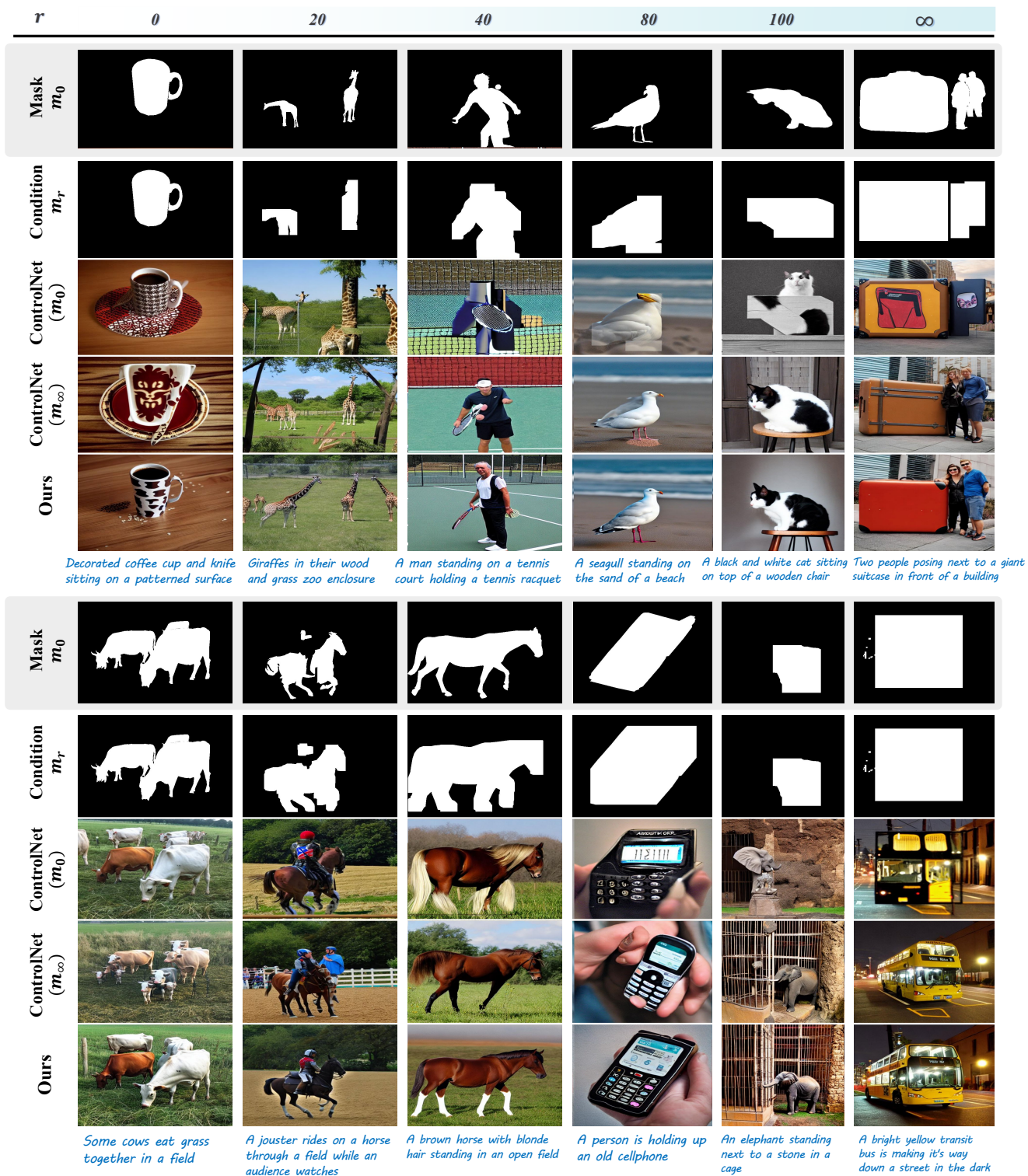


Figure 16: More examples of our Shape-aware ControlNet compared with the vanilla ControlNet, i.e., ControlNet- m_0 and ControlNet- m_∞ .

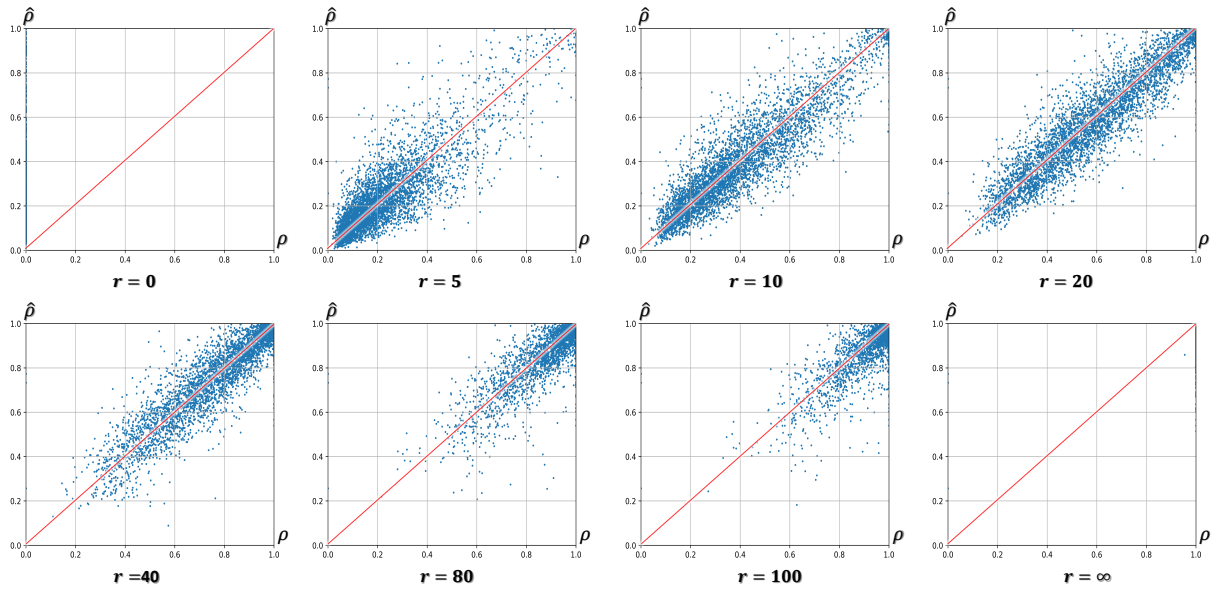


Figure 17: Error analysis of our deterioration estimator at different dilation radius r . The overall average $L1$ error is 5.47%. Notably, such errors show little impact on the performance of our Shape-aware ControlNet, referring to our main paper §6.3.

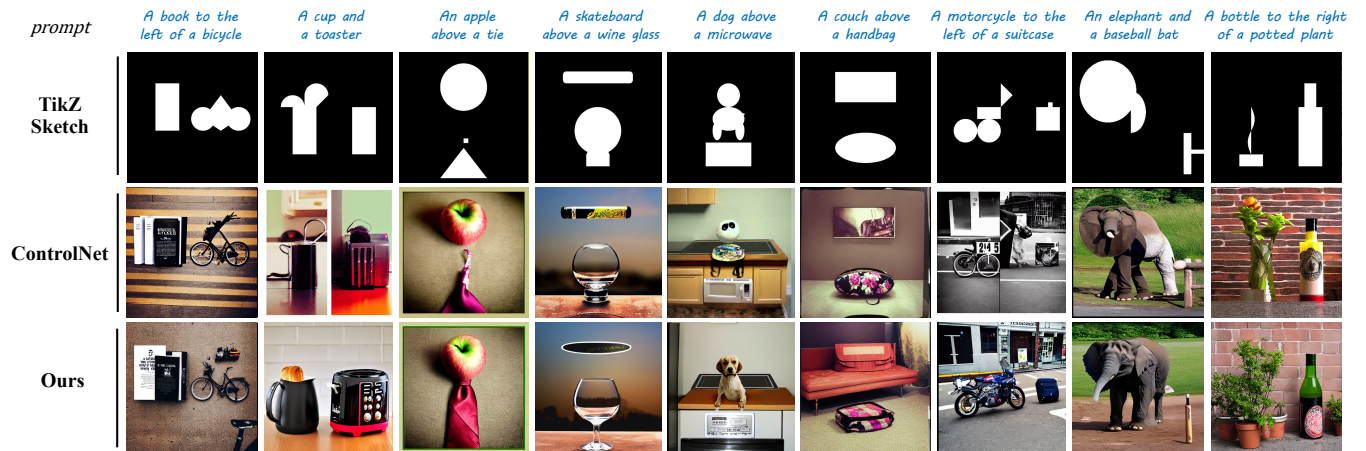


Figure 18: More examples of our method on TikZ sketches compared with the vanilla ControlNet. Our Shape-aware ControlNet exhibits advanced performance on generation with abstract masks with inaccurate contours.

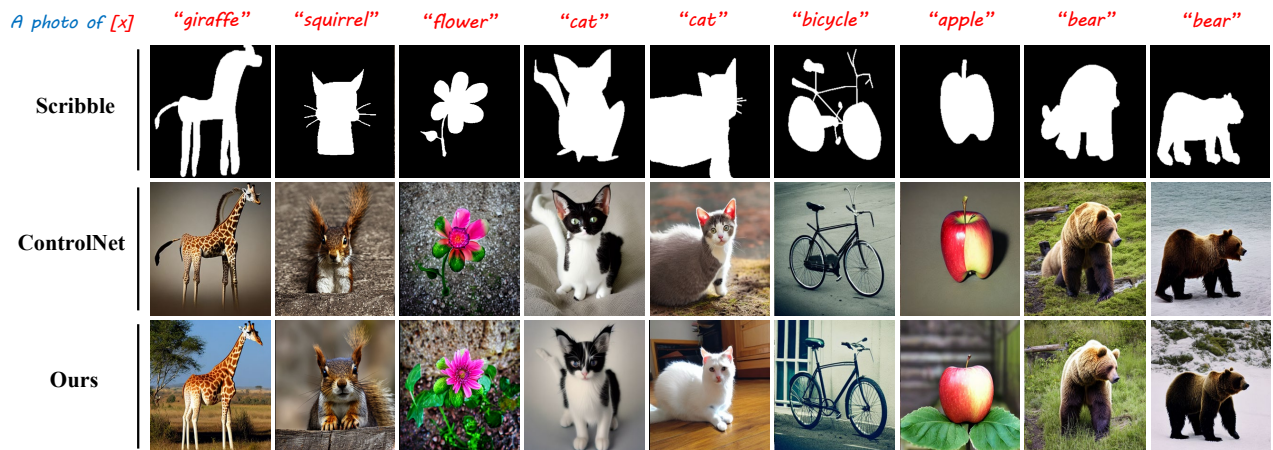


Figure 19: More examples of our method on human scribbles compared with the vanilla ControlNet. Our Shape-aware ControlNet exhibits advanced performance on generation with inexplicit masks with inaccurate contours.

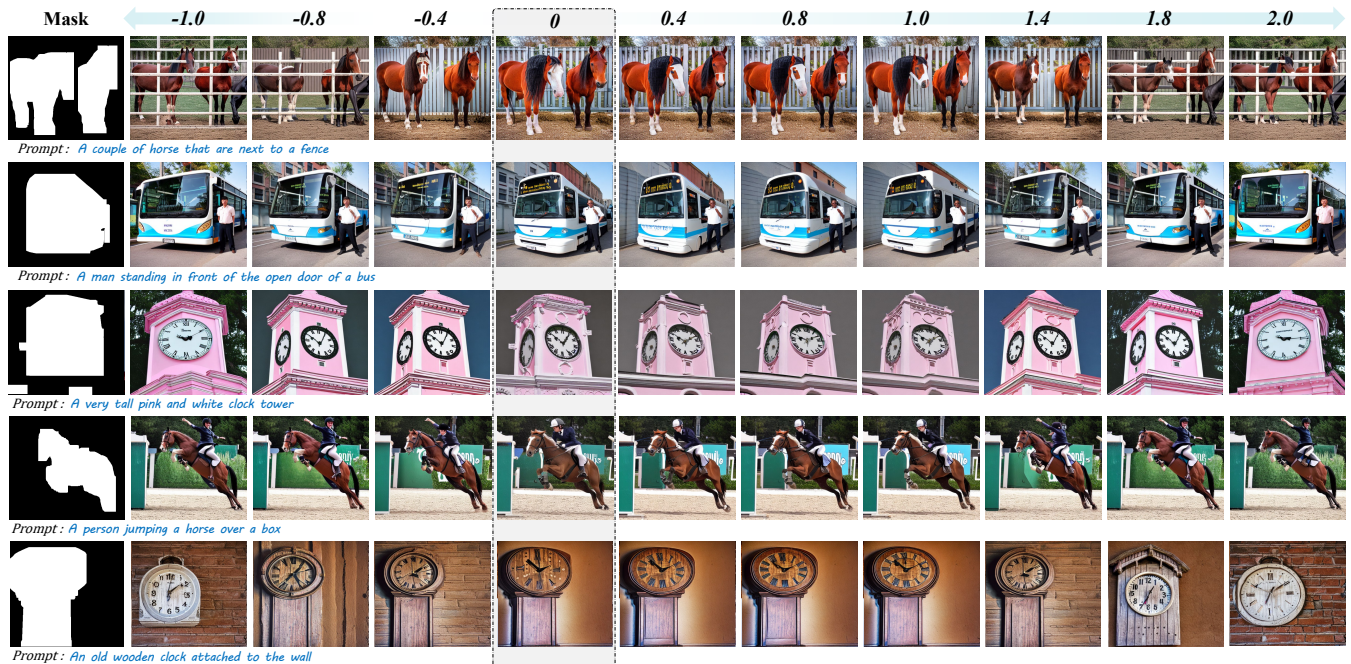


Figure 20: More examples of controlling object shape via the deterioration ratio ρ . Despite training with $\rho \in [0, 1]$, we empirically find it generalizes well to other values and offers additional control over the shape of generated objects. A small $|\rho|$ encourages generated objects to adhere more tightly to the outlines, and vice versa. Moreover, note that adjusting ρ has little impact on image fidelity.



Figure 21: More examples of composable shape-controllable generation with our method. Leveraging a Multi-ControlNet structure, we can assign different priors to each part of the control masks. This enables strict shape control over specific masks, while simultaneously allowing T2I diffusion models to unleash creativity in imagining objects of diverse shapes within inexplicit masks.